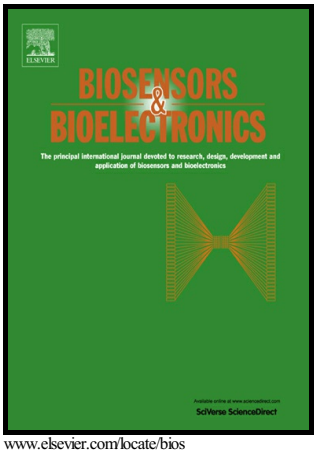

www.elsevier.com/locate/bios

A facile and green strategy for preparing newly-designed 3D graphene/gold film and its application in highly efficient electrochemical mercury assay

Lei Shi, Yan Wang, Shiming Ding, Zhenyu Chu, Yu Yin, Danfeng Jiang, Jingyi Luo, Wanqin Jin

PII: S0956-5663(16)30988-5
DOI: http://dx.doi.org/10.1016/j.bios.2016.09.104
Reference: BIOS9216

To appear in: *Biosensors and Bioelectronic*

Received date: 10 August 2016
Revised date: 27 September 2016
Accepted date: 28 September 2016

Cite this article as: Lei Shi, Yan Wang, Shiming Ding, Zhenyu Chu, Yu Yin, Danfeng Jiang, Jingyi Luo and Wanqin Jin, A facile and green strategy for preparing newly-designed 3D graphene/gold film and its application in highly efficient electrochemical mercury assay, *Biosensors and Bioelectronic* http://dx.doi.org/10.1016/j.bios.2016.09.104

A facile and green strategy for preparing newly-designed 3D graphene/gold film and its application in highly efficient electrochemical mercury assay

Lei Shi[a], Yan Wang[a], Shiming Ding[a*], Zhenyu Chu[b], Yu Yin[c], Danfeng Jiang[b], Jingyi Luo[b], Wanqin Jin[b]

[a]State Key Laboratory of Lake Science and Environment, Nanjing Institute of Geography and Limnology, Chinese Academy of Sciences, Nanjing 210008, P. R. China

[b]State Key Laboratory of Materials-Oriented Chemical Engineering, College of Chemical Engineering, Nanjing Tech University, Nanjing 210009, P. R. China

[c]School of Environmental and Chemical Engineering, Jiangsu University of Science and Technology, Zhenjiang 212003, P. R. China

[*]Corresponding Author. Tel: +86-25-86882207. Fax: +86-25-86882207. smding@niglas.ac.cn

Abstract

In this work, we report a facile and green strategy for in situ and one step preparation of a novel 3D graphene/gold (G/Au) film. Triggering with unique driving force from hydrothermal growth, a 3D interlaced graphene framework with hierarchically porous structures was directly attached on a gold substrate pretreated with a self-assembled monolayer. Simultaneously, highly dispersive Au nanoparticles with tunable morphologies were anchored on the framework

utilizing generated graphene as an endogenous reductant. Newly-designed 3D G/Au film possessed excellent properties of significantly large specific area, good electrical conductivity, high structure stability and substrate binding strength, etc. As a paradigm, an electrochemical Hg^{2+} biosensor was constructed on 3D G/Au film, in which an exonuclease III-assisted target recycling was introduced. Impressively, an ultralow detection limit of 50 aM (S/N=3), a wide linear range from 0.1 fM to 0.1 μM, a high selectivity and a good reliability for Hg^{2+} assay in real water and serum samples were realized using prepared biosensor. It is highly envisioned that this work opens the door towards simply fabricating varying types of 3D graphene based hybrid films, and such G/Au film will have widespread applications in electroanalysis and electrocatalysis.

Keywords

3D graphene/gold film; Hydrothermal growth; In situ preparation; Target recycling; Mercury sensing

1. Introduction

Due to highly toxic and bio-accumulative properties, mercury ion (Hg^{2+}) can impact human health and ecological environment even in trace amount (Jiang et al., 2006). Increasing attention has been focused on developing effective methods for Hg^{2+} detection (Aragay et al., 2011). Several analytical techniques have been established in the past few decades, including fluorescence and colorimetry (Kim et al., 2012; Xu et al., 2009a; Zhang and Chen, 2014), atomic absorption/emission spectroscopy (Erxleben and Ruzicka, 2005), and inductively coupled plasma mass spectrometry (ICP-MS) (Rahman et al., 2014). Although these techniques could determine

Hg^{2+} at low concentrations, they generally require expensive and sophisticated instrumentations. Comparatively, electrochemical methods have been widely introduced in Hg^{2+} assays, due to their great advantages of high sensitivity, low cost, and especially ease of miniaturization (Cui et al., 2015). For instance, anodic stripping voltammetry has been adopted to realize a sensitive and simultaneous assay of several metal ions. However, this method easily suffers from signal interferences of mutual ions, resulting in a poor selectivity in practice. Therefore, it is urgent to develop an electrochemistry based method with both high sensitivity and selectivity. Lately, it was revealed that T-T mismatches in DNA duplexes could selectively capture Hg^{2+} to form stable T-Hg^{2+}-T structures (Miyake et al., 2006). This interaction provides an opportunity for selective Hg^{2+} assays. Therefore, the combination of electrochemistry and biology opens new horizon for sensitive and selective Hg^{2+} detection (Kong et al., 2009; Wu et al., 2010; Zhang et al., 2013a; Zhuang et al., 2013).

Rapid development in the field of micro/nanomaterials creates prospective opportunities in designing promising electrochemical Hg^{2+} biosensors, in which emerging Au nanoparticles (AuNPs) have received special interest due to their unique physicochemical properties, e.g. a high surface-to-volume ratio and excellent biocompatibility (Saha et al., 2012; Tang et al., 2014; Zhu et al., 2009). Nevertheless, AuNPs easily aggregate owing to a high surface energy, resulting in a marked reduction in original availability. To overcome this obstacle, a plausible solution is to anchor AuNPs on specific support materials. Graphene, a one-atom-thick planar sheet densely packed with sp^2-bonded carbon atoms, has attracted considerable attention due to its excellent electrical conductivity, high flexibility and mechanical stability, large theoretical specific surface area and unique transport properties (Geim and Novoselov, 2007). In spite of these attractive properties, it is difficult to realize a chemical modification and immobilization of

biomolecules on graphene because of few available oxygenated functional groups, which limits its applications in the design of electrochemical biosensors (Chen et al., 2012). Consequently, effectively anchoring AuNPs on the graphene is highly anticipated to address the easy aggregation of AuNPs and improve the biocompatibility of graphene. Versatile graphene/gold (G/Au) hybrid materials have been prepared for many important applications, on account of their improved properties arising from the synergistic cooperation of individual materials (Niu et al., 2014; Tao et al., 2013; Turcheniuk et al., 2015). Apart from their use as bulk materials, constructing G/Au films on conductive substrates is prerequisite and stimulated by enormous demands in electronic and energy-related systems (Huang et al., 2012). As one frequently-used method, G/Au bulk materials were fabricated and subsequently transferred onto substrates to form films with a physical approach (Jang et al., 2015; Niu et al., 2014; Wang et al., 2011). This method seems simple, but as-prepared favourable structures of bulk materials may be destroyed and the binding strength on substrates is weak, leading to the easy peeling of films in usage. Alternatively, an electrochemical reduction (ER) or chemical vapour deposition (CVD) assisted method was proposed for constructing G/Au films on substrates, in which an improved binding strength was realized (Du et al., 2010; Tran Duy et al., 2016). Nevertheless, not only tedious steps are required but rarely 3D structures of graphene are obtained with the ER method. To our knowledge, 3D graphene structures are critical to realize a large accessible surface area and enable fast electron transport rate of graphene sheets (Li and Shi, 2012). Besides, CVD is complicated and technically demanding, hindering its widely practical applications. Therefore, it remains a great challenge to fabricate novel and desirable 3D G/Au films with facile approaches, which will open doors for advanced applications in electrochemical Hg^{2+} biosensing with significantly enhanced performance.

In addition, an effective Hg^{2+} sensing strategy is also crucial to improve its detectability, in which target recycling is regarded as a powerful strategy. Diverse nicking nucleases have been used for direct recycling of targets, resulting in remarkable signal amplification (Shi et al., 2014a; Zhu et al., 2012). Considering that nicking endonucleases suffer from the limitation in a specific recognition sequence, the exonuclease III (Exo III) is recommended and has been widely applied in detection of nucleic acid (Liu et al., 2015), bacteria (Luo et al., 2013) and small organic molecule (Hu et al., 2012). Recently, it was discovered that nicking reaction towards a DNA duplex with metal ion-mediated base pairing (e.g. T-Hg^{2+}-T) could also be realized with Exo III (Xuan et al., 2013), offering a potentiality to design novel sensing strategy to realize sensitive Hg^{2+} assays.

In this work, a facile and green strategy was demonstrated to realize in situ and one step preparation of desirable 3D G/Au films for the first time. Utilizing unique driving force from hydrothermal growth, graphene oxide was transformed into a 3D graphene framework which was tightly attached on self-assembled monolayer modified gold substrate. As the produced graphene could be employed as an endogenous reductant, simultaneous formation of AuNPs on the graphene framework occurred without any additional reductants. Superior properties of newly-designed 3D G/Au films on account of synergistic cooperation of graphene and AuNPs were explored, making them promising candidates in electroanalysis applications with high performance. As an example, an electrochemical Hg^{2+} biosensor with a strategy of Exo III-assisted target recycling was constructed on 3D G/Au film. Significantly enhanced response signals were produced, and a highly efficient assay of attomolar Hg^{2+} was realized with prepared biosensor.

2. Experimental section

2.1. Materials and reagents

See Supporting Information

2.2. In situ and one step fabrication of 3D G/Au films on gold substrates

Freshly pretreated gold substrate was immersed into a 4-aminothiophenol solution (0.5 mM) for 1 h to form a self-assembled monolayer (SAM). Graphene oxide (GO) was prepared by the oxidation of graphite powder according to a modified Hummers' method (Xu et al., 2009b). 20 mL precursor solution containing GO (2 mg/mL) and different concentrations of $HAuCl_4$ were sufficiently mixed. Then, SAM modified gold substrate was placed vertically into the solution and left at room temperature for 6 h, followed by heating in a Teflon-lined autoclave at 180°C for 6 h (Hu et al., 2012; Shi et al., 2014b). Coupling reagents of 2 mg EDC and 2 mg NHS were introduced to promote the condensation reaction between the $-NH_2$ groups of SAM and -COOH groups of GO. After the hydrothermal growth, the gold substrate was sufficiently washed with distilled water and treated with a freeze drying. 3D G/Au films prepared with different concentrations of $HAuCl_4$ were denominated as G/Au-0 (0 μM), G/Au-1 (10 μM), G/Au-2 (20 μM) and G/Au-3 (30 μM) respectively.

2.3. Construction of 3D G/Au film based electrochemical Hg^{2+} biosensor

R-probe/AuNPs conjugates were introduced to act as signal indicators for monitoring Hg^{2+} concentrations (Shi et al., 2013; Zhang et al., 2007). Briefly, 1 mL AuNPs were firstly centrifuged and the precipitates were resuspend in 1 mL phosphate buffered saline (PBS, pH 7.0,

10 mM). Then, 0.1 mL reporter probes (r-probes) in sterilized water with TCEP (10 mM) were added into 1 mL AuNPs solution and incubated at 4 °C for 16 h, in which the concentrations of r-probe I and r-probe II were 0.1 μM and 1 μM respectively. Then r-probe/AuNPs conjugates were aged by gradually adding NaCl (2 M) every 30 min to reach a final concentration of 0.1 M NaCl. The mixed solution was incubated for another 48 h and finally centrifuged for 30 min at 4 °C with the supernatant being removed. The red oily precipitate was washed with PBS, recentrifuged, and then redispersed in 1 mL PBS.

G/Au film modified gold substrate was immersed into an immobilization buffer (i-buffer, 10 mM Tris-HCl, 1 mM EDTA, 0.1 M NaCl, pH 7.0) containing capture probes (c-probes, 2 μM) and MCH (500 nM) with incubation time of 6 h, and unbound probes were sufficiently washed away with washing buffer (w-buffer, 10 mM Tris-HCl, pH 7.0). Then, the sensing interface was treated with Hg^{2+} at various concentrations for 0.5 h, again followed by thoroughly washing with the w-buffer. Subsquently, 1 μL Exo III (20 U/μL) was injected and the nicking reaction was implemented at 37 °C for 0.5 h. Finally, 0.1 mL conjugates of r-probe/AuNPs were added into the detection system and maintained for 2 h at 37 °C.

2.4. Electrochemical measurements

All electrochemical measurements were performed with a CHI 660E electrochemical workstation (Shanghai Chenhua, China). The three-electrode system consisting of 3D G/Au film modified working electrode, a platinum auxiliary electrode, and an Ag/AgCl (saturated KCl) reference electrode was used. Cyclic voltammetry (CV) was carried out at a scan rate of 100 mV/s, electrochemical impedance spectroscopy (EIS) was performed at frequencies from 0.01 Hz to 100 kHz with a 5 mV amplitude signal, and square wave voltammetry (SWV) was

implemented with a 10 mV amplitude signal at a frequency of 25 Hz. The electrolyte for CV was 10 mM $K_3Fe(CN)_6$ containing 3 M KCl unless specifically indicated, for EIS was 5 mM $K_3[Fe(CN)_6]/K_4[Fe(CN)_6]$ containing 0.1 M KCl, and for SWV was 10 mM PBS containing 0.25 M NaCl, in which deoxygenated distilled water was used for preparing these solutions.

3. Results and discussion

3.1. Fabrication and characterizations of 3D G/Au films

Preparation path of 3D G/Au films is illustrated in Fig. 1A. Au(III) ions were adsorbed on the highly negative-charged GO via partial replacement of Cl^- ligands (Ji et al., 2007), and acted as nucleation sites for the formation of AuNPs. Meanwhile, SAM modified gold substrate was employed for in situ growth of hybrid film. Treating with the hydrothermal reaction, GO was partially reduced into graphene and random stacking between flexible graphene sheets happened (Xu et al., 2010), resulting in a 3D graphene framework tightly attached on the substrate through the formation of −CO−NH− bonds. This chemical interaction was confirmed with characteristic vibrational peaks at around 1700 cm^{-1} (C=O stretch), 1585 cm^{-1} (an overlapped signature of the N−H and C=C bond) and 1225 cm^{-1} (C−N stretch) in FTIR (shown in Fig. S1A), and the appearance of N1s at 402 eV in XPS (Fig. S1B) (Mungse and Khatri, 2014). As produced graphene could be served as an endogenous reductant (Chen et al., 2011; Yin et al., 2012), simultaneous formation of AuNPs on the graphene surface was observed, realizing in situ and one step preparation of 3D G/Au film.

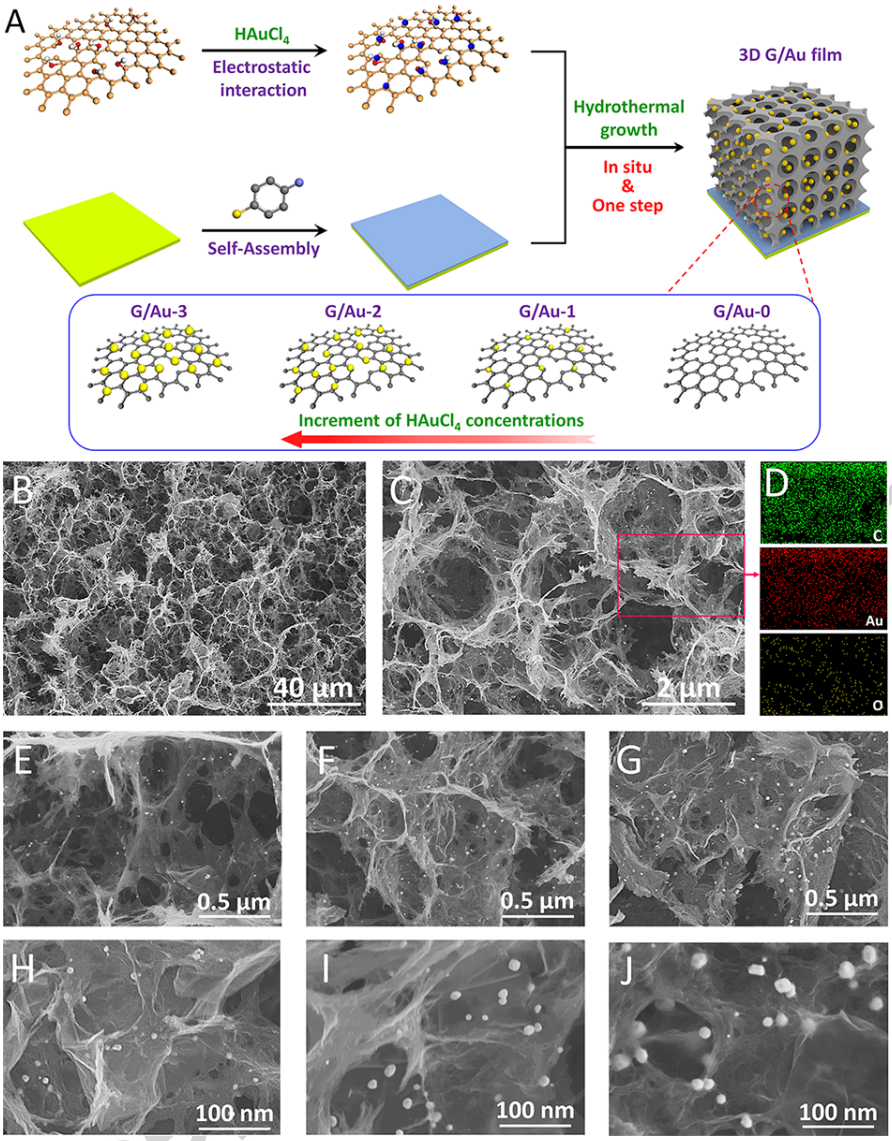

Fig. 1. (A) Preparation path of 3D G/Au film. (B), (C) FESEM images of G/Au films at low and high magnifications. (D) EDX mappings of C, Au and O element distribution respectively. FESEM images at low and high magnifications of (E), (H) G/Au-1 film, (F), (I) G/Au-2 film, (G), (J) G/Au-3 film.

As demonstrated in Fig. 1B, a large-scale and homogeneous 3D G/Au film was successfully prepared on the gold substrate, which possessed interconnected and hierarchically porous structures. Comparing with the G/Au-0 film (Fig. S2), the formation of AuNPs had no obviously effect on the morphology of prepared films. With a high magnification focused on the film

surface (Fig. 1C), a 3D graphene framework consisting of thin layers of stacked graphene sheets was produced, and AuNPs were uniformly dispersed on the framework, which was also proved in EDX mapping of Au element distribution (Fig. 1D). Besides, morphology evolutions of AuNPs on graphene were investigated by altering $HAuCl_4$ concentrations. As less nucleation sites were formed on GO at a low $HAuCl_4$ concentration (10 μM), AuNPs with a sparse density were produced on G/Au-1 film (Fig. 1E), and smaller AuNPs (~ 7 nm) were acquired (Fig. 1H). With an increased concentration of 20 μM, more Au(III) ions were adsorbed on GO and additional nucleation sites were generated. Accordingly, an obviously improved density of AuNPs on G/Au-2 was achieved (Fig. 1F), and AuNPs with enlarged diameters of ca. 12 nm were observed (Fig. 1I). While further increasing the concentration to 30 μM, no more nucleation sites were produced because of the saturation of adsorption sites on GO. Therefore, instead of a further improvement in the density of nanoparticles (Fig. 1G), significantly enlarged AuNPs (up to 25 nm) were produced on G/Au-3 (Fig. 1J). It is verified that 3D G/Au films were sucessfully prepared with the proposed strategy, and morphologies of AuNPs could be easily tuned through altering $HAuCl_4$ concentrations.

Several important merits are highly anticipated on newly-designed 3D G/Au films: (i) 3D hierarchically porous structure can provide a significantly large specific area and facilitate the mass transfer at interfaces; (ii) graphene framework consisting of thin layers of stacked graphene sheets will enable a fast electron transport; (iii) well dispersive AuNPs with tunable morphologies will extremely improve available catalysis and binding sites for molecules; (iv) excellent binding strength of hybrid films on substrates can be observed.

Obviously, in the absence of any additional reductants, a high purity accompanying with extraordinary properties would be observed on 3D G/Au films, which were investigated by XPS,

XRD and Raman respectively. As shown in Fig. 2A, comparing with GO consisting of C and O atoms, G/Au film was composed of C, O and Au atoms, as well as a small quantity of N and S atoms attributed to the SAM. After the hydrothermal reaction, peak intensity at 284.8 eV (C-C) significantly became stronger, together with the decrease of peaks at 286.6 (C-O), 288.0 (C=O), and 289.4 eV (O-C=O), as shown in Fig. 2B. It is indicated that effective removal of most oxygenated functional groups was realized, and atomic ratios of C1s/O1s increased from 2.1 to 6.2. As suggested in the inset in Fig. 2A, XPS signatures of Au 4f doublet ($4f_{7/2}$ and $4f_{5/2}$) belong to the reduced Au(0) particles (Negishi et al., 2005). There were red shifts in XPS peaks of AuNPs compared with bulk Au (83.8 eV), which are typical for small metal particles on support materials and attributed to reduced core-hole screening in metal clusters (Senz et al., 2009). This result highlights that electronic properties of produced AuNPs would be significantly different from bulk materials.

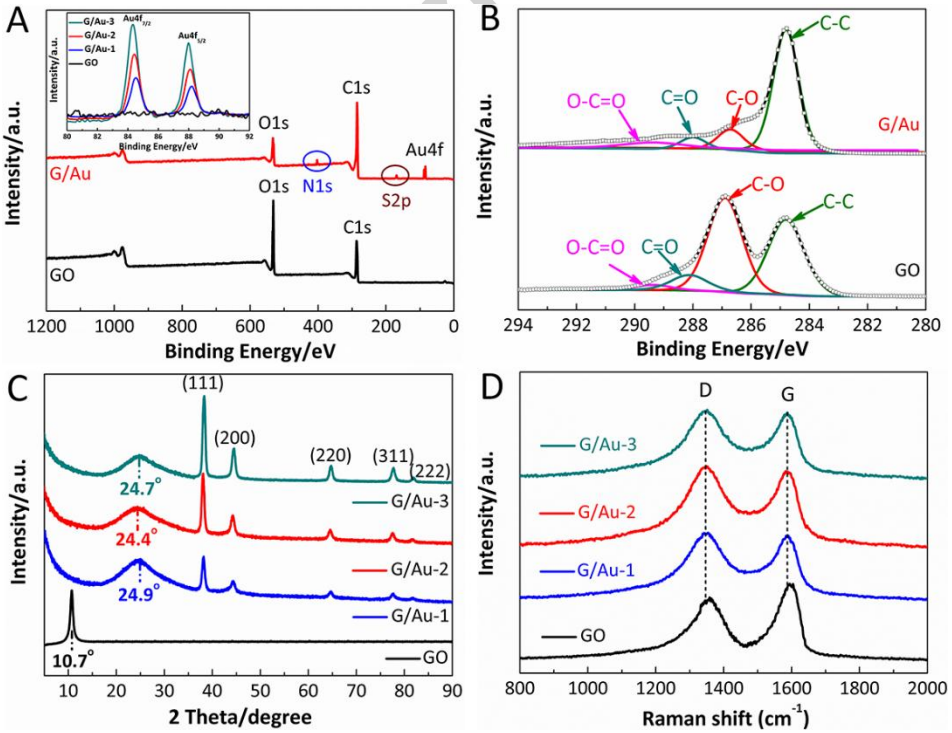

Fig. 2. (A) XPS survey scan spectra of GO and G/Au film, inset was the XPS spectra of AuNPs. (B) The C1s XPS spectra of GO and G/Au film. (C) XRD patterns, and (D) Raman spectra of GO and G/Au films.

XRD patterns of 3D G/Au films are shown in Fig. 2C. Comparing with a sharp peak of GO (10.7^o), broad XRD peaks of G/Au films at ca. 24.5^o are assigned to poorly ordered graphene sheets along their stacking direction and reflect that graphene sheets are few-layer stacked, which is consistent with results observed in FESEM. Meanwhile, the characteristic peaks at 38.1^o (111), 44.2^o (200), 64.5^o (220), 77.6^o (311) and 81.7^o (222) belong to face-centered cubic crystalline Au. The intensity ratios of the (111) to (200) diffraction line (2.1 of G/Au-1, 2.4 of G/Au-2, 2.6 of G/Au-3) are higher than that of the standard diffraction of Au powder (1.9), showing that AuNPs on graphene had a tendency to grow with the lowest energy surface (Shi et al., 2015). Besides, from results of XPS and XRD, it is found that residual oxygenated functional groups remained on G/Au films, which was also demonstrated in EDX mapping of O element distribution in Fig. 1D. These hydrophilic groups would enable a favorable interaction and improve the recognition efficiency towards biological molecules in aqueous solutions. Furthermore, Raman spectra displayed a D-band at around 1350 cm^{-1} and a G-band at 1590 cm^{-1} are shown in Fig. 2D. The I_D/I_G is calculated to be ca. 1.02 (G/Au-1, G/Au-2) and 1.01 (G/Au-3) respectively (slightly higher than 0.85 on GO), indicating the creation of new quasi-amorphous sp^2-bonded carbons upon hydrothermal growth, and the formation of AuNPs introduced very few defects on graphene. Moreover, the D- and G-bands in G/Au films exhibits a small red shift compared with that of GO, suggesting a potential interaction between graphene and AuNPs (Subrahmanyam et al., 2010).

3.2. Electrochemical characterizations of 3D G/Au films

CV tests were introduced to investigate electrochemical properties of 3D G/Au films, as shown in Fig. 3A. In contrast to a low signal of the substrate (5.8 μA), obviously increased oxidation peak currents from 20.7 μA (G/Au-0), 31.7 μA (G/Au-1), 45.3 μA (G/Au-2) to 49.5 μA (G/Au-3) were obtained. Comparing with a large peak current change from G/Au-1 to G/Au-2 (13.6 μA), a decreased change (4.2 μA) was observed from G/Au-2 to G/Au-3 due to enlarged AuNPs (Fig. 3B). Accompanying with increased peak currents, remarkably decreased peak potential differences (ΔE_p) from 96.2 mV (substrate), 80.1 mV (G/Au-0), 74.3 mV (G/Au-1), and 70.0 mV (G/Au-2) to 72.4 mV (G/Au-3) with a maximum at G/Au-2 were acquired. The possible reason is attributed to that heterojunctions of AuNPs/graphene serve as favorable electron transfer channels (Ho et al., 2015), while AuNPs with increased diameters prolong the electron transfer path to the heterojunctions. As smaller ΔE_p values indicate fast electron transfer rates, the formation of AuNPs on a 3D graphene framework not only improves the specific surface area, but significantly enhances the electrical conductivity on accounts of the synergistic cooperation. In addition, 3D G/Au films were consecutively scanned for 100 cycles to assess the structure stability and binding strength on substrates (Fig. S3). As shown in Fig. 3C, acceptable current changes within 4.1% were observed on G/Au films, revealing that not only an excellent structure stability but high substrate binding strength was achieved. Meanwhile, EIS was adopted to investigate the electron transfer resistance (R_{et}) of different G/Au films. As shown in Fig. 3D, comparing with a relatively large R_{et} of 22.3 Ω on gold substrate, smaller semicircles of 17.1 Ω on G/Au-0, 12.7 Ω on G/Au-1, 7.2 Ω on G/Au-2, and 7.1 Ω on G/Au-3 were obtained respectively. The formation of G/Au films obviously reduces R_{et} values due to their large specific

area and high electrical conductivity, which facilitate the mass exchange and electron transfer at interfaces.

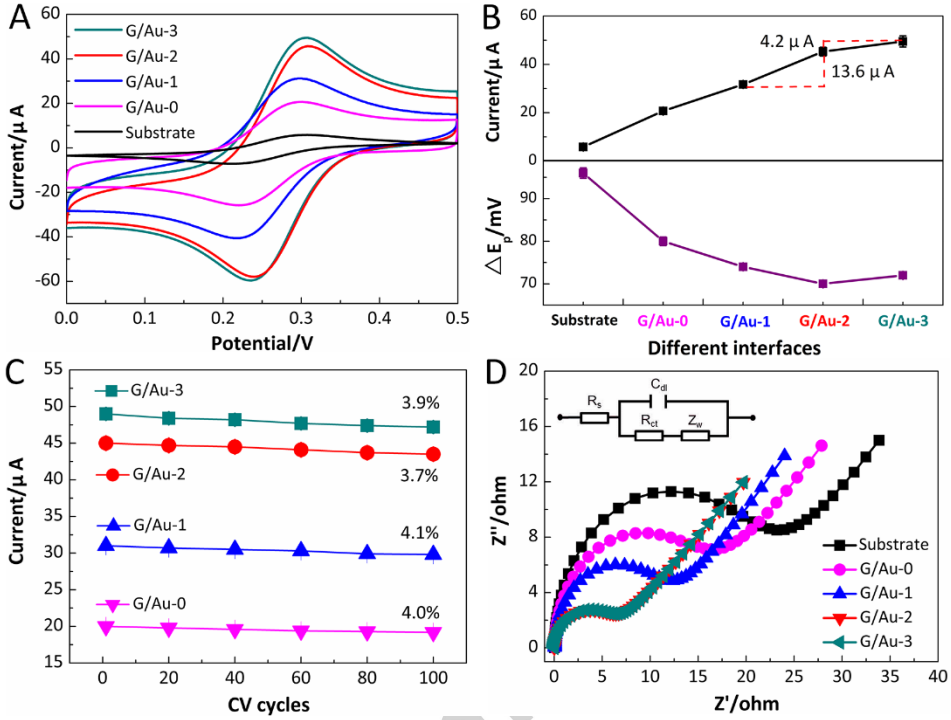

Fig. 3. (A) CV, and (B) Corresponding oxidation peak currents and ΔE_p of G/Au films. (C) Peak currents of G/Au films recorded during 100 consecutive CV measurements. (D) EIS tests of G/Au films.

In brief, newly-designed 3D G/Au films prepared with a facile and green strategy, were demonstrated to possess superior properties due to the synergistic cooperation of graphene and AuNPs, e.g. significantly large surface area, excellent electrical conductivity, high structure stability and substrate binding strength, and good biocompatibility. All of these merits would make them promising candidates in the applications of electrochemical Hg^{2+} biosensing with high performance.

3.3. Designing Hg^{2+} detection strategy on prepared 3D G/Au film

Due to a relatively large specific area and high electrical conductivity, G/Au-2 film was selected for the construction of the Hg^{2+} biosensor, as illustrated in Fig. 4. Firstly, c-probes with stem-loop structrues were covalently attached to G/Au film, leaving free T bases at 3' termini for binding with Hg^{2+}. In the presence of Hg^{2+}, available T bases were tightly paired through the formation of T-Hg^{2+}-T, leading to the formation of nicking sites. Up on the addition of Exo III, nicking reaction was motivated and the step-wise removal of mononucleotides from the 3' termini was realized. As a result, stem segments of c-probes were digested and residual c-probes were available to hybridize with r-probe I in r-probe/AuNPs. Subsequently, Hg^{2+} was dissociated and reused to produce more T-Hg^{2+}-T structures, triggering next nicking cycle and resulting in numerous residual c-probes. Finally, r-probe/AuNPs was added and the resulting signal was used to indicate Hg^{2+} concentrations.

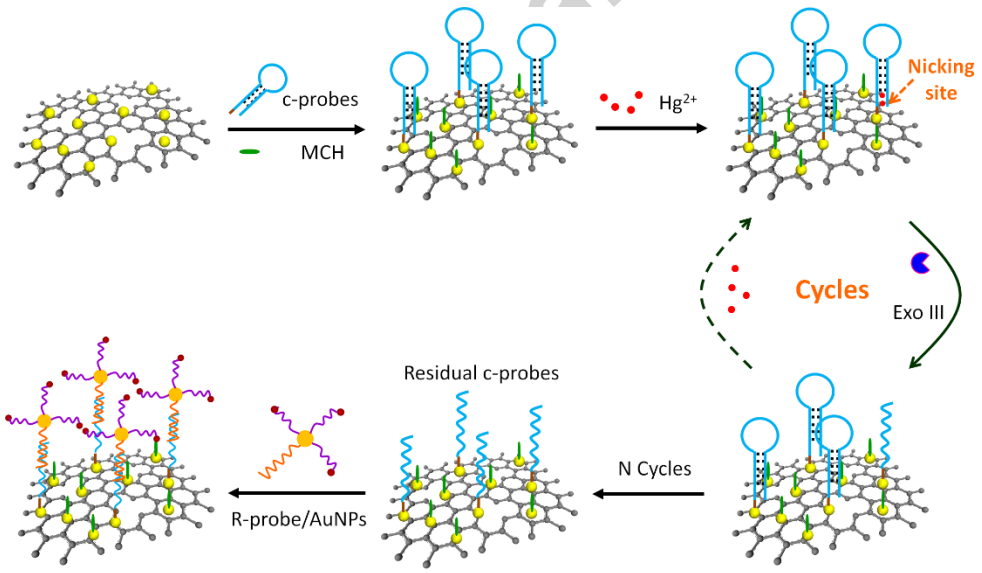

Fig. 4. Schematic illustration of 3D G/Au film based electrochemical Hg^{2+} biosensor with an Exo III-assisted recycling strategy.

3.4. Electrochemical investigations of designed Hg^{2+} biosensor

EIS was introduced to investigate impedance changes at different interfaces (Fig. 5A). In comparison with a small semicircle of G/Au-2 film, a significantly increased R_{et} was observed after incubating with c-probes and MCH (curve a), which was attributed to the electrostatic repulsion of oligonucleotide strands and steric hindrance from the stem-loop structures and MCH (Steel et al., 1998). Subsequently, electrostatic repulsion was slightly declined due to the formation of T-Hg^{2+}-T structures, resulting in a subtle decrease in R_{et} (curve b). Upon the addition of Exo III, stem segments of c-probes were digested, resulting in an apparent decrease in impedance semicircle (curve c). Finally, improved steric hindrance and electrostatic repulsion were produced after hybridizing with r-probe/AuNPs, forming a remarkably increased R_{et} (curve d). In contrast, impedance changes in the absence of Hg^{2+} were also investigated. As the nicking reaction was not activated, negligible changes in R_{et} were observed (Fig. S4A). Moreover, SWV was introduced to monitor the responses in Hg^{2+} detection (Fig. 5B), due to its excellent resolution of the electrochemical signals in similar sensing systems (Kang et al., 2009). Comparing with a low signal in the absence of Hg^{2+} (2.5 μA, curve a), a significantly enhanced signal (26.2 μA, ca. 10.5-fold, curve b) was observed at a low concentration of 1 nM Hg^{2+}, showing that designed sensing scheme was feasible in Hg^{2+} detection. Besides, a subtle response was observed at 1 nM Hg^{2+} without the Exo III (Fig. S4B), indicating that Exo III was essential to digest c-probes and realize the Hg^{2+} recycling. Similarly, CV was also implemented to monitor response changes, and results were consistent with those in SWV, as shown in Fig. S4C.

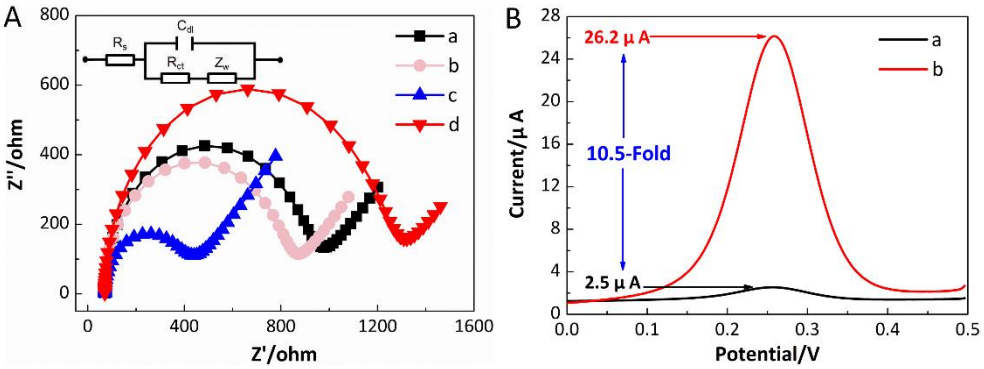

Fig. 5. (A) Nyquist plots of the biosensor at different interfaces, (a) c-probes and MCH immobilized G/Au, (b) in the presence of Hg^{2+}, (c) after the addition of Exo III, (d) in the presence of r-probe/AuNPs. (B) SWV of the biosensor, (a) in the absence of Hg^{2+}, (b) in the presence of 1 nM Hg^{2+}.

3.5. Optimization of experimental conditions on response signals

Effect of experimental conditions on response signals was investigated. Signal changes (Δi) of the biosensor at varying incubation time of c-probes are depicted in Fig. S5A. It is found that a higher value of 23.7 μA was obtained at 6 h, in which a proper density of c-probes were created. Meanwhile, as T becomes quaternized at low pH values and Hg^{2+} precipitates form at high pH values (Wang et al., 2016), a sensitive response of 23.7 μA at pH 7.0 was observed (Fig. S5B). Subsequently, the dosages of Exo III were studied at a high Hg^{2+} concentration of 0.1 μM, as shown in Fig. S5C. The Δi increased rapidly with more Exo III and reached a saturation value of 28.3 μA at 20 U, verifying that 20 U Exo III was adequate in the sensing system. Moreover, nicking time was explored to obtain a high signal (Fig. S5D). Treating with an ultralow Hg^{2+} concentration of 0.1 fM, Δi reached a saturation value within 30 min. As less nicking time was necessary at higher Hg^{2+} concentrations, optimal nicking time of 30 min was introduced in subsequent tests.

3.6. Performance of fabricated electrochemical Hg^{2+} biosensor

Sensitivity and linear range of the biosensor were further investigated by varying Hg^{2+} concentrations. As shown in Fig. 6A, enhanced response signals were generated with increasing Hg^{2+} concentrations from 0 aM to 10 μM, because additional residual c-probes were produced for hybridizing with r-probe/AuNPs. The linear relationship between Δi and the logarithm of Hg^{2+} concentrations was obtained in the range from 0.1 fM to 0.1 μM on the G/Au-2 film (Fig. 6B), and a regression equation of $\Delta i=46.15+2.62\cdot \mathrm{Log}C_{Hg}{}^{2+}$ ($R^2=0.996$) was calculated, in which an ultralow detection limit of 50 aM (S/N=3) was observed. Each point of the calibration curve was performed in quintuplicate, and the maximum relative standard deviation (RSD) was 5.10%, which guaranteed a high precision of the biosensor. Furthermore, standard samples containing different Hg^{2+} concentrations were tested with ICP-MS and prepared biosensor respectively. As shown in Table S1, the obtained results were basically the same, ensuring a good reliability of the biosensor. Although more assay time was consumed comparing with some other T-Hg^{2+}-T based electrochemical biosensors (Table S2), the performance of prepared biosensor was superiorly better than those of reported ones. Besides, the preparation strategy for constructing desirable G/Au films was more facile and efficient, which would facilitate their applications in practice and realize high-performance and reliable assays. (Chen et al., 2014; Kong et al., 2009; Li et al., 2016; Shi et al., 2014a; Wang et al., 2016; Wu et al., 2016; Zhang et al., 2013a; Zhang et al., 2013b; Zhuang et al., 2013). In addition, similar Hg^{2+} assays based on G/Au-1, G/Au-3 and gold substrate were also investigated (Fig. 6C). Under the same condition, lower sensitivities of 2.53, 2.17 and 1.44 with higher detection limits of 0.5 fM, 3 fM and 0.2 nM were observed on G/Au-3, G/Au-1 and gold substrate respectively. As expected, G/Au-2 film possesses a better performance than those of other G/Au films. Especially, the detection limit of G/Au-2 film based

biosensor is over 7 orders of magnitude lower than that of gold substrate, confirming that superior properties of 3D G/Au play a critical role in the ultrasensitive Hg^{2+} detection.

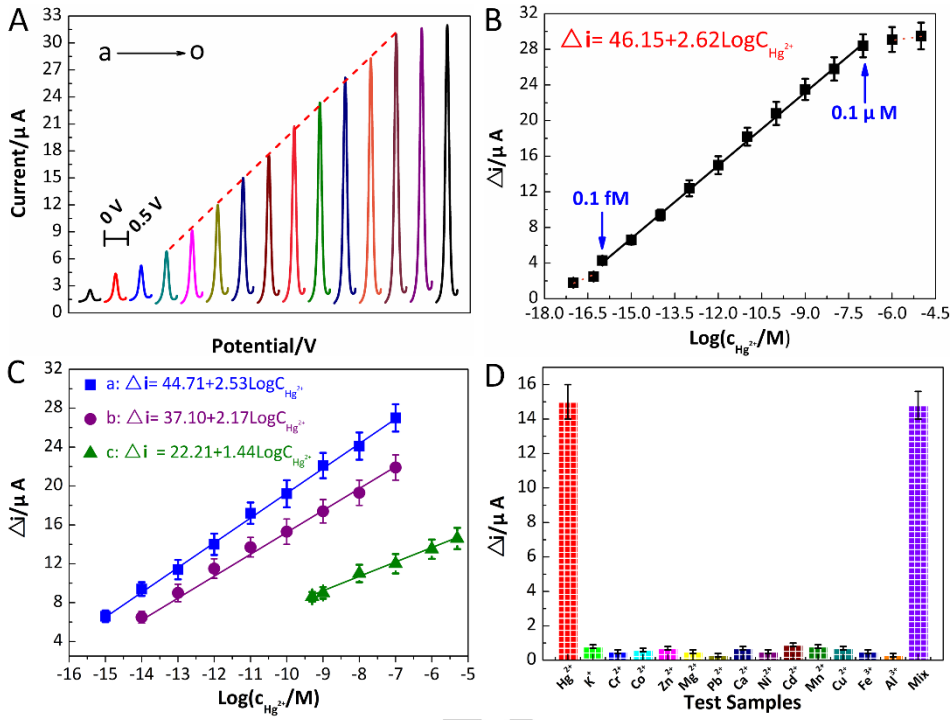

Fig. 6. (A) SWV of the biosensor at different Hg^{2+} concentrations, from (a) to (o) were 0, 10 aM, 50 aM, 0.1 fM, 1 fM, 10 fM, 0.1 pM, 1 pM, 10 pM, 0.1 nM, 1 nM, 10 nM, 0.1 μM, 1 μM and 10 μM respectively. (B) Calibration curve of Δi with logarithm of Hg^{2+} concentrations based on G/Au-2 film. (C) Calibration curves of Δi with logarithm of Hg^{2+} concentrations based on (a) G/Au-3, (b) G/Au-1 and (c) gold substrate respectively. (D) Selectivity of prepared Hg^{2+} biosensor.

Selectivity of the biosensor was explored by monitoring the Δi with other common metal ions. The solutions tested included 1 pM Hg^{2+}, 1 mM each metal ion, and a mixture of the two. Comparing with Δi of 1 pM Hg^{2+}, the biosensor showed negligible responses to 1 mM other metal ions (Fig. 6D), indicating a satisfactory selectivity was obtained on the biosensor. In addition, an excellent reproducibility and high stability were also observed on prepared biosensor, as shown in Fig. S6.

3.7. Practical applications in real water and serum samples

The Hg^{2+} assay in real samples of lake water, tap water and human serum was studied respectively. To ensure the comparability of our biosensor with ICP-MS, lake water samples were first treated with a UV digestion and acidification to liberate Hg^{2+} from other species. As Hg^{2+} concentration in tap water and human serum was below the detection limit of prepared biosensor, the standard addition method was employed. As shown in Table S3, it is found that Hg^{2+} concentrations determined by our biosensor were in good agreement with ICP-MS or standard additions, confirming that prepared biosensor was reliable for Hg^{2+} detection in real samples.

4. Conclusions

In summary, we have successfully established a facile and green strategy for in situ and one step preparation of desirable 3D G/Au films for the first time. Newly-designed 3D G/Au films were demonstrated to possess superior properties due to the synergistic cooperation of graphene and AuNPs, making them promising candidates in electrochemical sensing to achieve high performance. As a selected example, an ultrasensitive electrochemical Hg^{2+} biosensor with a strategy of Exo III-assisted target recycling was constructed on 3D G/Au film. It is highly envisioned that our proposed strategy will provide new insight into the design of more 3D graphene based hybrid films, and the as-synthesized 3D G/Au films would open up wide horizon for electroanalysis and electrocatalysis applications.

Acknowledgements

This work was supported by the National Natural Science Foundation of China (Nos. 41322011, 41571465, 21607159), the Natural Science Foundation of Jiangsu Province (No. BK20161087), the National High-level Personnel of Special Support Program and Nanjing Institute of Geography and Limnology, CAS (NIGLAS2015QD07).

References

Aragay, G., Pons, J., Merkoci, A., 2011. Chem. Rev. 111, 3433-3458.

Chen, D., Feng, H.B., Li, J.H., 2012. Chem. Rev. 112, 6027-6053.

Chen, J., Tang, J., Zhou, J., Zhang, L., Chen, G., Tang, D., 2014. Anal. Chim. Acta 810, 10-16.

Chen, X., Wu, G., Chen, J., Chen, X., Xie, Z., Wang, X., 2011. J. Am. Chem. Soc. 133, 3693-3695.

Cui, L., Wu, J., Ju, H., 2015. Biosens. Bioelectron. 63, 276-286.

Du, M., Yang, T., Jiao, K., 2010. J. Mater. Chem. 20, 9253-9260.

Erxleben, H., Ruzicka, J., 2005. Anal. Chem. 77, 5124-5128.

Geim, A.K., Novoselov, K.S., 2007. Nat. Mater. 6, 183-191.

Ho, P.-H., Liou, Y.-T., Chuang, C.-H., Lin, S.-W., Tseng, C.-Y., Wang, D.-Y., Chen, C.-C., Hung, W.-Y., Wen, C.-Y., Chen, C.-W., 2015. Adv. Mater. 27, 1724-1729.

Hu, C.G., Zhao, Y., Cheng, H.H., Wang, Y.H., Dong, Z.L., Jiang, C.C., Zhai, X.Q., Jiang, L., Qu, L.T., 2012. Nano Lett. 12, 5879-5884.

Huang, X., Zeng, Z., Fan, Z., Liu, J., Zhang, H., 2012. Adv. Mater. 24, 5979-6004.

Jang, H.D., Kim, S.K., Chang, H., Choi, J.H., Cho, B.G., Jo, E.H., Choi, J.W., Huang, J.X., 2015. Carbon 93, 869-877.

Ji, X., Song, X., Li, J., Bai, Y., Yang, W., Peng, X., 2007. J. Am. Chem. Soc. 129, 13939-13948.

Jiang, G.B., Shi, J.B., Feng, X.B., 2006. Environ. Sci. Technol. 40, 3672-3678.

Kang, D., Zuo, X.L., Yang, R.Q., Xia, F., Plaxco, K.W., White, R.J., 2009. Anal. Chem. 81, 9109-9113.

Kim, H.N., Ren, W.X., Kim, J.S., Yoon, J., 2012. Chem. Soc. Rev. 41, 3210-3244.

Kong, R.-M., Zhang, X.-B., Zhang, L.-L., Jin, X.-Y., Huan, S.-Y., Shen, G.-L., Yu, R.-Q., 2009. Chem. Commun., 5633-5635.

Li, C., Shi, G., 2012. Nanoscale 4, 5549-5563.

Li, Z.B., Miao, X.M., Xing, K., Peng, X., Zhu, A.H., Ling, L.S., 2016. Biosens. Bioelectron. 80, 339-343.

Liu, S.F., Cheng, C.B., Liu, T., Wang, L., Gong, H.W., Li, F., 2015. Biosens. Bioelectron. 63, 99-104.

Luo, C., Tang, H., Cheng, W., Yan, L., Zhang, D., Ju, H., Ding, S., 2013. Biosens. Bioelectron. 48, 132-137.

Miyake, Y., Togashi, H., Tashiro, M., Yamaguchi, H., Oda, S., Kudo, M., Tanaka, Y., Kondo, Y., Sawa, R., Fujimoto, T., Machinami, T., Ono, A., 2006. J. Am. Chem. Soc. 128, 2172-2173.

Mungse, H.P., Khatri, O.P., 2014. J. Phys. Chem. C 118, 14394-14402.

Negishi, Y., Nobusada, K., Tsukuda, T., 2005. J. Am. Chem. Soc. 127, 5261-5270.

Niu, Z., Liu, L., Zhang, L., Shao, Q., Zhou, W., Chen, X., Xie, S., 2014. Adv. Mater. 26, 3681-3687.

Rahman, G.M.M., Wolle, M.M., Fahrenholz, T., Kingston, H.M.S., Pamuku, M., 2014. Anal. Chem. 86, 6130-6137.

Saha, K., Agasti, S.S., Kim, C., Li, X., Rotello, V.M., 2012. Chem. Rev. 112, 2739-2779.

Senz, V., Fischer, T., Oelssner, P., Tiggesbaeumker, J., Stanzel, J., Bostedt, C., Thomas, H., Schoeffler, M., Foucar, L., Martins, M., Neville, J., Neeb, M., Moeller, T., Wurth, W., Ruehl, E., Doerner, R., Schmidt-Boecking, H., Eberhardt, W., Gantefoer, G., Treusch, R., Radcliffe, P., Meiwes-Broer, K.H., 2009. Phys. Rev. Lett. 102.

Shi, L., Chu, Z., Liu, Y., Jin, W., 2015. J. Mater. Chem. B 3, 3134-3140.

Shi, L., Chu, Z., Liu, Y., Jin, W., Chen, X., 2013. Biosens. Bioelectron. 49, 184-191.

Shi, L., Chu, Z., Liu, Y., Jin, W., Chen, X., 2014a. Biosens. Bioelectron. 54, 165-170.

Shi, L., Chu, Z., Liu, Y., Jin, W., Xu, N., 2014b. Adv. Funct. Mater. 24, 7032-7041.

Steel, A.B., Herne, T.M., Tarlov, M.J., 1998. Anal. Chem. 70, 4670-4677.

Subrahmanyam, K.S., Manna, A.K., Pati, S.K., Rao, C.N.R., 2010. Chem. Phys. Lett. 497, 70-75.

Tang, S., Tong, P., Lu, W., Chen, J., Yan, Z., Zhang, L., 2014. Biosens. Bioelectron. 59, 1-5.

Tao, Y., Lin, Y., Huang, Z., Ren, J., Qu, X., 2013. Adv. Mater. 25, 2594-2599.

Tran Duy, T., Balamurugan, J., Hwang, J.Y., Kim, N.H., Lee, J.H., 2016. Carbon 98, 90-98.

Turcheniuk, K., Boukherroub, R., Szunerits, S., 2015. J. Mater. Chem. B 3, 4301-4324.

Wang, N., Lin, M., Dai, H.X., Ma, H.Y., 2016. Biosens. Bioelectron. 79, 320-326.

Wang, Y., Zhang, S., Du, D., Shao, Y., Li, Z., Wang, J., Engelhard, M.H., Li, J., Lin, Y., 2011. J. Mater. Chem. 21, 5319-5325.

Wu, D., Wang, Y.G., Zhang, Y., Ma, H.M., Pang, X.H., Hu, L.H., Du, B., Wei, Q., 2016. Biosens. Bioelectron. 82, 9-13.

Wu, D.H., Zhang, Q., Chu, X., Wang, H.B., Shen, G.L., Yu, R.Q., 2010. Biosens. Bioelectron. 25, 1025-1031.

Xu, X.W., Wang, J., Jiao, K., Yang, X.R., 2009a. Biosens. Bioelectron. 24, 3153-3158.

Xu, Y., Sheng, K., Li, C., Shi, G., 2010. ACS Nano 4, 4324-4330.

Xu, Y., Zhao, L., Bai, H., Hong, W., Li, C., Shi, G., 2009b. J. Am. Chem. Soc. 131, 13490-13497.

Xuan, F., Luo, X., Hsing, I.M., 2013. Anal. Chem. 85, 4586-4593.

Yin, H., Tang, H., Wang, D., Gao, Y., Tang, Z., 2012. ACS Nano 6, 8288-8297.

Zhang, J., Song, S., Wang, L., Pan, D., Fan, C., 2007. Nat. Protoc. 2, 2888-2895.

Zhang, R.Z., Chen, W., 2014. Biosens. Bioelectron. 55, 83-90.

Zhang, Y., Zhao, H., Wu, Z., Xue, Y., Zhang, X., He, Y., Li, X., Yuan, Z., 2013a. Biosens. Bioelectron. 48, 180-187.

Zhang, Z., Yin, J., Wu, Z., Yu, R., 2013b. Anal. Chim. Acta 762, 47-53.

Zhu, Z., Gao, F.L., Lei, J.P., Dong, H.F., Ju, H.X., 2012. Chem. Eur. J. 18, 13871-13876.

Zhu, Z., Su, Y., Li, J., Li, D., Zhang, J., Song, S., Zhao, Y., Li, G., Fan, C., 2009. Anal. Chem. 81, 7660-7666.

Zhuang, J., Fu, L., Tang, D., Xu, M., Chen, G., Yang, H., 2013. Biosens. Bioelectron. 39, 315-319.

Highlights

- A facile and green strategy is established to prepare novel 3D G/Au films.
- Unique driving force for film preparation stems from hydrothermal reduction.
- Newly-designed 3D G/Au films possess significantly improved properties.
- An Exonuclease III-assisted Hg^{2+} recycling strategy is designed.
- An electrochemical biosensor for attomolar Hg^{2+} assay is constructed.

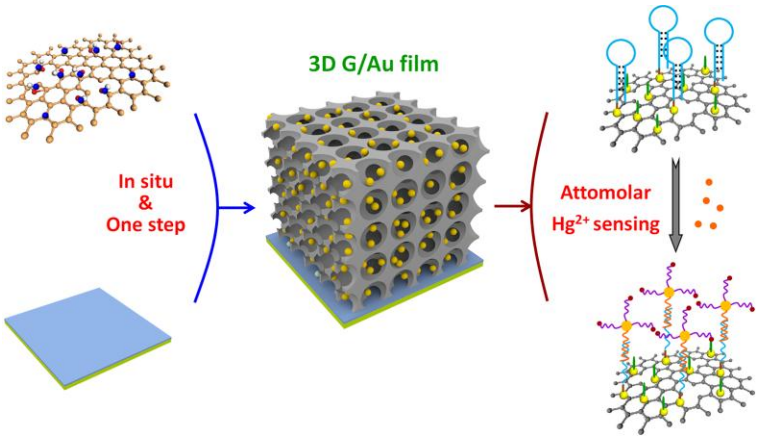

Graphical Abstract